Target Acceleration Estimation in Active and Passive Radars

Karol Abratkiewicz, *Member, IEEE*, Mateusz Malanowski, *Senior Member, IEEE*, and Zbigniew Gajo

***Abstract*—Flying targets are becoming increasingly maneuverable, contributing to the growing problem of their detection with active and passive radars. Rapid acceleration causes blurring of the target echo on the range-Doppler (RD) map, which reduces the signal-to-noise ratio in a given range and velocity cell. This article proposes a novel, nonparametric approach to quickly and efficiently estimating target acceleration on the RD map. In this article, a universal signal model for an active frequency-modulated continuous wave radar and a passive radar is introduced. Based on this model, an estimation algorithm has been developed that can be applied to both active and passive radars. Compared with the method known from the literature, the proposed solution is much faster (even more than 100 times) while maintaining numerical stability and allowing for the estimation of acceleration of many targets to be performed simultaneously. The proposed method was supported by simulation tests and signals from real-life active and passive radars observing a jet fighter and a drone. The obtained outcomes show that the proposed technique can be successfully used for autonomous real-time systems that detect and estimate the parameters of maneuvering vehicles.**

***Index Terms*—Acceleration estimation, active radar, passive radar, radar remote sensing, target detection.**

I. Introduction

NOWADAYS, one can find aerial vehicles with extreme maneuverability, such as drones [1], [2], [3], [4], jets or aircrafts [5], [6], rockets [7], and warheads [8]. Giving unique abilities to flying targets is particularly important on the battlefield as it allows such targets to avoid attacks by rapid acceleration and changes in flight direction. As maneuvering abilities increase, so does the need for systems capable of estimating target movements in order to detect and track them [2]. The flying target kinetic parameters are usually estimated by radars that have the ability to work during the day and night and are capable of operating in almost all weather conditions, such as rain, snow, and fog [9]. These advantages of radars over other systems, e.g., visual or acoustical systems, are the reason they are commonly used today. In addition to the widespread use of active radars, passive radars that use existing radiation sources to imaging and detect targets (e.g., television or radio signals) [9], [10], [11], [12], [13], [14], [15], [16] are becoming more significant.

Manuscript received 13 May 2023; revised 26 August 2023; accepted 19 September 2023. Date of publication 27 September 2023; date of current version 13 October 2023. *(Corresponding author: Karol Abratkiewicz.)*

The authors are with the Institute of Electronic Systems, Warsaw University of Technology, 00-665 Warsaw, Poland (e-mail: karol.abratkiewicz@pw.edu.pl; mateusz.malanowski@pw.edu.pl; zbigniew.gajo@pw.edu.pl).

Digital Object Identifier 10.1109/JSTARS.2023.3319829

The problem of detecting fast objects has often been raised in the literature. For high-speed targets with constant velocity, the so-called stretch processing was proposed, concentrating the echo coming from the object by appropriately manipulating the reference signal and increasing the integration gain [17]. As a result, one can obtain a clear echo without a spread along the range and Doppler axis. The problem is more complex for maneuvering objects because it requires taking into account the next degree of freedom in the motion model, which are acceleration or higher order movement parameters [18]. Several attempts to deal with this issue can be found in the literature. A typical approach to address the problem of acceleration estimation is to compute a 3-D distribution comprising the range, velocity, and acceleration [5], [7], [19], [20], [21]. Iterative computing of multiple range-Doppler (RD) maps with a modulated reference signal according to an assumed acceleration accomplishes this. However, this technique has significant drawbacks, the greatest of which is the enormous computational cost. In the case of real-time applications, the method may turn out to be too complex, as the number of required RD maps can be in the region of several thousand. Targets, such as jets or maneuvering warheads, can speed up considerably. In the case of passive radars, where one works with bistatic geometry, the accelerations in such a coordinate system may be more complicated, which increases the computational effort because the algorithm searches the entire set of analyzed accelerations in order to find the optimum [20]. Another problem is the need to initially know the velocity and range of the target in order to narrow down the analysis only to a given area. Otherwise, an adaptive 3-D search of the space for target detection is necessary, further increasing the computational burden. The acceleration of a given target may be outside the scanned area. Then, the precise estimation is not possible. The greatest advantage of the technique based on a 3-D RD-acceleration distribution is its accuracy, which is somewhat equivalent to matched filtering, thanks to which the optimal signal-to-noise ratio (SNR) is obtained at the output. However, a significant need to develop a nonparametric method of estimating acceleration in radars is desired due to the computational cost of the known methods [5].

In other works, the problem is considered from different perspectives. For instance, in [22], the authors proposed an algorithm for the motion parameter estimation of moving targets in a multistatic passive radar. This approach, however, requires several transmitting or receiving stations, increasing the system's complexity. Similarly, in [23], the radar network was used to estimate uniformly accelerating target parameters; however,

the work is devoted only to the forward scattering scenario. There are also other methods of estimating the parameters of target movement. One of them is the Keystone transform [24], but its disadvantage is computational cost, the inability to process signals with some spatial Doppler frequencies, and echo migration between spatial Doppler bands for high-maneuvering targets. In [25], the authors used Lv's distribution [26] to estimate target kinematic parameters. However, the authors consider the presence of unknown additive white Gaussian noise without additional interference and clutter, which cannot always hold true in practice. Moreover, the technique was tested using simulations without real-life validation. The Hough and polynomial chirplet transforms were used for the estimation of target parameters in [27]. The main limitation of this technique is the prerequisite that the targets have different motion parameters. Otherwise, its precise estimation is impeded, if possible at all. All of the mentioned methods have some limitations and assumptions and, what is tangible in the light of this article, are designed to work with a given type of radar (passive or active). The outperformance resulting from the ability to migrate the method between different systems, and its versatility would bring tremendous benefits in practical system realization and efficient implementation.

This article is focused on a low-cost method for estimating the acceleration of a noncooperative vehicle in monostatic active frequency modulated continuous wave (FMCW) radars and single-node passive radars. The aim of the study was to develop an unsupervised algorithm capable of determining target kinetic parameters with low computational effort. The in-depth research was inspired by works devoted to time–frequency (TF) analysis [28] and the mutual relationship between the cross-ambiguity function (CAF) used in radars and the short-time Fourier transform (STFT) [29], [30]. As shown in this article, some properties of the TF distribution can be used in signal parameter estimation from the RD map. However, in contrast to TF techniques, the research presented here, first, deals with 2-D signals that do not appear in the TF analysis; second, it applies the concept to RD radar processing that, to the best of authors' knowledge, has never been used in this way.

The rest of this article is organized as follows. Section II presents the assumptions, fundamentals, and derivations of the proposed method. Next, in Section III, the implementation details are provided. Section IV briefly describes the reference method to which the outcomes are compared. In Sections V and VI, the simulation and real-life signal analysis results are shown, respectively. The application of the proposed method to integration time elongation in passive radar is illustrated in Section VII. Finally, Section VIII concludes this article.

II. Derivations

In this section, derivations of the novel acceleration estimators are provided. First, the signal model for active FMCW and passive radars is presented. Next, the unified range-compressed distribution is defined for both of these radars. On this basis, the acceleration estimators are proposed.

A. Assumptions

Let us assume a unified kinematic model of a moving target. In both monostatic and bistatic cases, for the accelerating object at the initial range R_0, velocity V_0, and acceleration A_0, the target-radar range is a function of time

$$R(t) = R_0 + V_0 t + \frac{A_0 t^2}{2}. \tag{1}$$

It has to be highlighted that for a monostatic scenario (considered as an active radar in this article), parameters R_0, V_0, and A_0 are viewed as their radial components. The same quantities describe bistatic target kinematic attributes for the bistatic case (passive radar) [31], [32]. For a short observation period, the range $R(t)$ can be assumed to be constant, and the resulting baseband signal delay reaching the receiver can also be approximated to be constant. As a result, the target echo is analyzed as if it only occupies a single range cell (range migration does not occur). Further considerations are carried out assuming the constant signal delay so that it obeys (for c expressing the speed of light)

$$\tau = \frac{M \cdot R(t)}{c} \approx \text{const.} \tag{2}$$

where M is a coefficient equal to 1.0 for bistatic (passive) and 2.0 for monostatic (FMCW) radar. The above assumption allows for neglecting range migration and preserves the general concept presented in this article.

B. Signal Model

1) FMCW Radar: Let us assume a complex transmitted signal model given as

$$x_T(t) = \mathscr{A}_T(t) e^{j\left(\phi_i + \omega_c t + \frac{\alpha t^2}{2}\right)},\ 0 < t < T_{\text{sweep}} \tag{3}$$

where $\mathscr{A}_T(t)$ is the amplitude (presented as a varying function to express its real-life nature, where the radio part usually affects the output signal envelope), T_{sweep} is a sweep time, $j = \sqrt{-1}$, ϕ_i is the initial phase, $\omega_c = 2\pi f_c$ is the angular frequency with a carrier frequency f_c, and α is the chirp rate. Signal (3) is called *sweep* and is periodically emitted by the radar. For the stationary single-point target, the received signal is given as

$$x_R(t) = \mathscr{A}_R(t-\tau) e^{j\left(\phi_r + \omega_c(t-\tau) + \frac{\alpha(t-\tau)^2}{2}\right)} \tag{4}$$

where $\mathscr{A}_R(t)$ is the received signal envelope delayed concerning the target distance and scaled according to its radar cross section [31], and ϕ_r is the constant phase of the reflected signal resulting from signal propagation and target reflectivity. Both signals $x_T(t)$ and $x_R(t)$ are mixed in the receiver, which yields

$$\begin{aligned} x_{B,s}(t) &= x_T^*(t) \cdot x_R(t) \\ &= \mathscr{A}_T^*(t)\mathscr{A}_R(t-\tau) e^{j\phi_0 - j\frac{\alpha t^2}{2} + j\frac{\alpha t^2 - 2t\tau\alpha + \alpha\tau^2}{2} - j\omega_c\tau} \\ &= \mathscr{A}_T^*(t)\mathscr{A}_R(t-\tau) e^{j\left(\phi_0 + \frac{\alpha\tau^2}{2} - \frac{2t\tau\alpha}{2} - \omega_c\tau\right)} \end{aligned} \tag{5}$$

where subscript B, s comes from *baseband* and *stationary*. $\phi_0 = \phi_i - \phi_r$ is the initial phase difference between the transmitted and the received signals and, together with $\omega_c\tau$, are constant and

can be neglected. Let us assume that the envelope $\mathscr{A}_T^*(t)\mathscr{A}_R(t-\tau)$ in (5) takes on the form $\mathscr{A}_{B,s}(t)$, which is the amplitude of the mixed signal comprising the transmitted and received envelopes. Also, $\frac{\alpha\tau^2}{2} \approx 0$, thus for the stationary target, one has

$$x_{B,s}(t) \approx \mathscr{A}_{B,s}(t)e^{-j\omega_b t} \tag{6}$$

where $\omega_b = \tau\alpha = \frac{2R\alpha}{c}$ is the beat angular frequency, and where R is the range from the radar to the target. For moving targets, the Doppler phase shift in the receiver depends on the wavelength λ. If the target moves with a velocity V, the received signal is modulated according to the Doppler angular frequency

$$\omega_D = 2\pi f_D = -2\pi\frac{2V}{\lambda}. \tag{7}$$

Also, for acceleration A, the second-order term appears in the received signal phase, giving a frequency modulation (FM) term as follows [33]:

$$\vartheta = -2\pi\frac{A}{\lambda}. \tag{8}$$

Thus, for the accelerating target, (6) can be rewritten as

$$x_{B,a}(t) = \mathscr{A}_{B,s}(t)e^{j\left((\omega_D-\omega_b)t+\frac{\vartheta t^2}{2}\right)} \tag{9}$$

where subscript B, a denotes *baseband* and *acceleration*. Signal (9) is then processed in the receiver.

2) Passive Radar: Passive radars use signals of opportunity to illuminate targets. Let us assume a signal with a varying phase $\phi(t)$ and a carrier angular frequency ω_c

$$x_T(t) = \mathscr{A}_T(t)e^{j(\phi(t)+\omega_c t)}. \tag{10}$$

Analogously to the FMCW radar, for the accelerating target, the received signal can be given as

$$x_R(t) = \mathscr{A}_R(t-\tau)e^{j\left(\phi(t-\tau)+\phi_0+(\omega_c+\omega_D)t+\frac{\vartheta t^2}{2}\right)} \tag{11}$$

and is then further processed. In (11), ϕ_0 is a constant phase change due to the wave traveling through space and the target's reflection coefficient. This parameter does not affect further analysis. For bistatic radars, the received Doppler angular frequency is slightly different than (7) and according to the assumption in Section II-A is given as

$$\omega_D = 2\pi f_D = -2\pi\frac{V}{\lambda}. \tag{12}$$

The signals in passive radar are continuous and cannot be divided into pulses or sweeps. However, it is possible to introduce a time duality analogous to a conventional pulse radar. The authors propose the 2-D representations (distributions) of the transmitted and received signals, respectively

$$\begin{aligned} X_T(t,t') &= \delta(t+t') * x_T(t) \\ &= \mathscr{A}_T(t+t')e^{j(\phi(t+t')+\omega_c(t+t'))}, \quad t' \geq 0, t \geq 0 \end{aligned} \tag{13}$$

$$\begin{aligned} X_R(t,t') &= \delta(t+t') * x_R(t) \\ &= \mathscr{A}_R(t+t'-\tau)e^{j\left(\phi(t+t'-\tau)+(\omega_c+\omega_D)(t+t')+\frac{\vartheta(t+t')^2}{2}\right)} \\ & t' \geq 0, t \geq 0. \end{aligned} \tag{14}$$

where $\delta(t)$ is the Dirac delta, $\mathscr{A}_R(t)$ is the received signal envelope delayed and weakened according to the target range and radar cross section, and $*$ denotes the convolution operator. The notation proposed in (13) and (14) is a straightforward and continuous-time interpretation of the so-called batches algorithm commonly used in passive radars [34]. The interpretation can be summarized as follows. The transmitted and received signals are divided into smaller parts (batches), which can be expressed as their delay according to the slow time (convolution with a Dirac delta function). As a result, both signals form 2-D distributions whereby the first dimension t corresponds to signal samples (fast time), and the second one represents consecutive batches (slow time).

C. Range Compression

1) FMCW Radar: In FMCW radars, the range compression is performed as a Fourier transform of each demodulated pulse. Hence, the operation can be interpreted as an STFT with no window overlap

$$\mathcal{R}_T(t,\omega) = \int_{\mathbb{R}} x_{B,a}(\tau)g(\tau-t)e^{-j\omega\tau}\mathrm{d}\tau \tag{15}$$

where ω is directly linked with the range r, and $g(t)$ is a real and even analyzing window. The signal (9) can be written as

$$x_{B,a}(t) = \mathscr{A}_{B,s}(t)e^{j2\pi\Phi(t)} \tag{16}$$

where $\Phi(t)$ is a quadratic polynomial. Using Taylor series expansion of $\Phi(t)$ around point u, we obtain

$$x_{B,a}(t) = \mathscr{A}_{B,s}(t)e^{j2\pi\left(\Phi(u)+\Phi'(t-u)+\frac{1}{2}\Phi''(t-u)^2\right)}. \tag{17}$$

For sufficiently small $|t-u|$ being small enough, one can assume that $\mathscr{A}_{B,s}(t) \approx \mathscr{A}_{B,s}(u)$ and (17) can be written as

$$x_{B,a}(t) = x_{B,s}(u)e^{j2\pi\left(\Phi'(u)(t-u)+\frac{1}{2}\Phi''(u)(t-u)^2\right)}. \tag{18}$$

Now, according to the results presented in [35], the STFT (15) with the Gaussian window $g(t) = e^{-\pi t^2}$ is given by

$$\mathcal{R}_T(t,\omega) = x_{B,a}(t)m^{-\frac{1}{2}}e^{-j\frac{\theta}{2}}e^{-\frac{\pi(1+j\Phi''(t))(\omega-\Phi'(t))^2}{1+\Phi''(t)}} \tag{19}$$

where $m = \sqrt{1+\vartheta^2}$ and $\theta = \tan^{-1}(-\vartheta)$. Since (2) assumes a short observation time, so that $R(t) \approx$ const., $\Phi'(t)$ and $\Phi''(t)$ tend to 0. Also, for the FMCW radar, the angular frequency of the beat signal and range are associated as $\omega_b = \frac{2r\alpha}{c}$, and $\omega_D - \omega_b \approx -\omega_b$ (because $\omega_b \gg \omega_D$). Thus, the range–time distribution can be defined as

$$\mathcal{R}_T(t,r) \approx m^{-\frac{1}{2}}e^{-j\frac{\theta}{2}}x_{B,s}(t)e^{j\left(-\pi\left(\frac{2r\alpha}{c}\right)^2-\frac{2r\alpha}{c}t+\frac{\vartheta t^2}{2}\right)}. \tag{20}$$

Without loss of generality, the envelope can be assumed to be a bivariate Gaussian bell function

$$\mathscr{A}(t,r) = \mathcal{A}e^{-\frac{(t-t_x)^2}{2\sigma_t^2}-\frac{(r-r_x)^2}{2\sigma_r^2}} \tag{21}$$

with the standard deviation in range and time σ_r and σ_t, respectively. Such an assumption simplifies (20) to the following form:

$$\mathcal{R}_T(t,r) = \mathcal{A}e^{-\frac{(t-t_x)^2}{2\sigma_t^2}-\frac{(r-r_x)^2}{2\sigma_r^2}} e^{j\left(\left(-\pi\left(\frac{2r\alpha}{c}\right)^2-\frac{\theta}{2}\right)-\frac{2r\alpha}{c}t+\frac{\vartheta t^2}{2}\right)}. \tag{22}$$

Equation (22) is the distribution in the range–time domain. However, our interest is to find the chirp rate along the time direction; thus, r is not considered. Assuming $a_0 = -\pi\left(\frac{2r\alpha}{c}\right)^2 - \frac{\theta}{2}$, $a_1 = -\omega_b = \frac{2r\alpha}{c}$, and $a_2 = \vartheta$, we get

$$\mathcal{R}_T(t,r) = \mathscr{A}(t,r)e^{j\left(a_0+a_1t+\frac{a_2t^2}{2}\right)}. \tag{23}$$

As can be seen, the range–time signal distribution is the windowed chirp whose chirp rate results from the target acceleration.

2) Passive Radar: Let us define an autocorrelation function for the transmitted signal as

$$\mathcal{C}_T(t,r) = \int_{\mathbb{R}} X_T(t,t')X_T^*\left(t,t'-\frac{r}{c}\right)\mathrm{d}t'. \tag{24}$$

The function depends on time t, as the calculation can start in different time moments. The function also depends on the range r, which corresponds to the time delay. The autocorrelation function reaches its maximum for $r = 0$. The shape of the function depends on the analyzed signal $x_T(t',t)$. In practice, the main lobe of the autocorrelation function is relatively constant; however, the sidelobes fluctuate due to the random nature of the signal.

Let us now define a cross-correlation function of the transmitted $X_T(t,t')$ and received $X_R(t,t')$ signals

$$\mathcal{R}_T(t,r) = \int_{\mathbb{R}} X_R(t,t')X_T^*\left(t,t'-\frac{r}{c}\right)\mathrm{d}t'. \tag{25}$$

Substituting (14) and (13) into (25) leads to

$$\begin{aligned}\mathcal{R}_T(t,r) &= \int_{\mathbb{R}} X_R(t,t')X_T^*\left(t,t'-\frac{r}{c}\right)\mathrm{d}t' \\ &= \int_{\mathbb{R}} \mathscr{A}_R\left(t+t'-\frac{r}{c}\right)e^{j\left(\phi\left(t+t'-\frac{r}{c}\right)+(\omega_c+\omega_D)(t+t')+\frac{\vartheta(t+t')^2}{2}\right)} \\ &\quad\times \mathscr{A}_T\left(t+t'\right)e^{-j\left(\phi\left(t+t'-\frac{r}{c}\right)+\omega_c\left(t+t'-\frac{r}{c}\right)\right)}\mathrm{d}t' \\ &= \underbrace{e^{j\left(\omega_c\frac{r}{c}+\omega_D t+\frac{\vartheta t^2}{2}\right)}}_{\text{phase modulation}} \underbrace{\int_{\mathbb{R}} \mathscr{A}_R\left(t+t'-\frac{r}{c}\right)\mathscr{A}_T\left(t+t'\right)\mathrm{d}t'}_{\text{real-value envelope correlation}} \\ &\quad\times \underbrace{\int_{\mathbb{R}} e^{j\left(\omega_D t'+\frac{\vartheta 2tt'+\vartheta t'^2}{2}\right)}\mathrm{d}t'}_{\approx 1}.\end{aligned} \tag{26}$$

The cross correlation (26) is composed of three factors. The first one is responsible for phase modulation according to the target velocity and acceleration. The second one results from correlating the real-value signal envelopes and does not affect the distribution phase as it is also real valued. The last term has a marginal influence on the estimation capabilities since the phase is random and close to 0, and the entire factor tends to be 1 due to the short observation time t'. For simplicity, one can assume that the range–time distribution envelope can be modeled as a bivariate Gaussian function

$$\mathscr{A}(t,r) = \mathcal{A}e^{-\frac{(t-t_x)^2}{2\sigma_t^2}-\frac{(r-r_x)^2}{2\sigma_r^2}}. \tag{27}$$

Then, the signal model for passive radar after range compression becomes

$$\mathcal{R}_T(t,r) = \mathcal{A}e^{-\frac{(t-t_x)^2}{2\sigma_t^2}-\frac{(r-r_x)^2}{2\sigma_r^2}} e^{j\left(a_0+a_1t+\frac{a_2t^2}{2}\right)} \tag{28}$$

which, in principle, is very similar to the FMCW case, and where $a_0 = \omega_c\frac{r}{c}$, $a_1 = \omega_D$, and $a_2 = \vartheta$.

To support the range–time signal model derived in (26), let us present a simulated passive radar scenario for an accelerating target illuminated by the DVB-T signal with a carrier frequency of $f_c = 680$ MHz and a bandwidth of $B = 7.6$ MHz. The transmitter location is not crucial from the perspective of acceleration estimation and is neglected in the analysis. The simulated target was observed for $T_i = 0.5$ s at the bistatic range of 4 km and had the initial velocity $V = -10$ m/s and acceleration $A = -30$ m/s^2. The results are shown in Fig. 1. Fig. 1(a) illustrates the magnitude of the range–time distribution. For the entire integration time, the target echo correlated with the reference signal forms a bell-shaped envelope across the range [see the second factor in (25)]. For the range cell where the target echo is located, the phase along time t is shown in Fig. 1(b). The result of a nonlinear function coincides with the first factor in (26). The last component of (26) with a negligible influence on the further considerations is shown in Fig. 1(c). The phase varies randomly with a mean close to 0.

The example shown in Fig. 1(a) also clarifies why approximation (27) holds true. In the range direction, the echo can be understood as a Gaussian bell with a small time spread parameter $\sigma_t \to 0$, whereas in the slow time direction, one can see a Gaussian bell with a large spread $\sigma_r \to \infty$. This assumption is also essential for active radar cases, where the same model was derived in (21).

D. Acceleration Estimation

For the range–time distribution model given as

$$\mathcal{R}_T(t,r) = \mathcal{A}e^{-\frac{(t-t_x)^2}{2\sigma_t^2}-\frac{(r-r_x)^2}{2\sigma_R^2}} e^{j\left(a_0+a_1t+\frac{a_2t^2}{2}\right)} \tag{29}$$

one has

$$\frac{\partial\mathcal{R}_T(t,r)}{\partial t} = (qt+p)\mathcal{R}_T(t,r) \tag{30}$$

where $q = -\frac{1}{\sigma_t^2} + ja_2$ and $p = \frac{t_x}{\sigma_t^2} + ja_1$.

A typical radar signal processing consists of Fourier transform computation along the time axis, which gives a RD distribution as

$$\begin{aligned}\mathcal{D}^h(v,r,t) &= \mathcal{F}_{t\to v}\{\mathcal{R}_T(t,r)\} \\ &= \int_{\mathbb{R}} \mathcal{R}_T(\eta,r)h(\eta-t)e^{-jv\eta}\mathrm{d}\eta \\ &= e^{-jvt}\int_{\mathbb{R}} \mathcal{R}_T(\eta-t,r)h(\eta)e^{jv\eta}\mathrm{d}\eta\end{aligned} \tag{31}$$

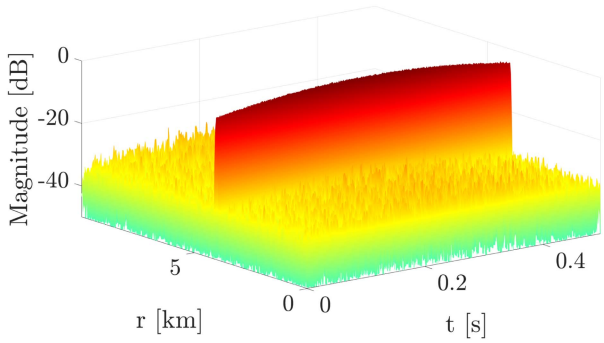

(a)

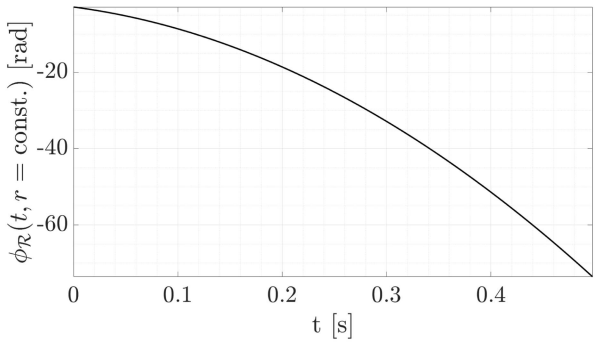

(b)

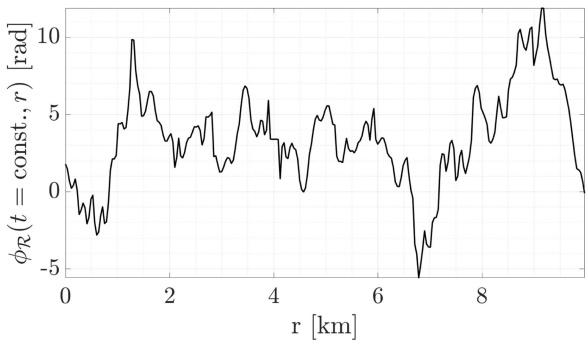

(c)

Fig. 1. Range–time distribution and its phase for cross sections for $r = \text{const.}$ and $t = \text{const.}$ (a) Simulated range–time distribution for a passive radar. (b) Range–time distribution phase for $r = \text{const.}$ (c) Range–time distribution phase for $t = \text{const.}$

where $h(t)$ is a differentiable window as a function of slow time. Equation (31) is a 3-D distribution in the general case. However, the last dimension (time t) reflects consecutive integration time instants. For a single RD map, this parameter can be neglected, and in the further part of this article, single-snapshot RD maps are analyzed, yielding a 2-D distribution. As a result, further considerations use $\mathcal{D}^h(v, r)$ instead of $\mathcal{D}^h(v, r, t)$.

Differentiating (31) with respect to time once leads to

$$\mathcal{D}^{h'}(v,r) = \frac{\partial \mathcal{D}^h}{\partial t}(v,r) = \int_{\mathbb{R}} \mathcal{R}_T(\eta, r)\frac{\mathrm{d}h}{\mathrm{d}t}(\eta - t)e^{-jv\eta}\mathrm{d}\eta$$

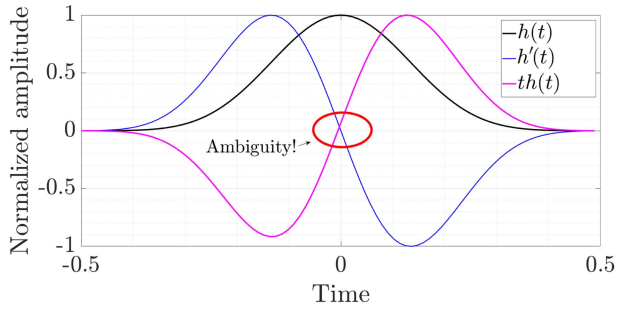

Fig. 2. Ambiguity effect for the differentiated window and the window multiplied by the time ramp.

$$= -jv\mathcal{D}^h(v,r) - e^{-jvt}\int_{\mathbb{R}} \frac{\partial \mathcal{R}_T}{\partial t}(\eta - t, r)h(\eta)e^{jv\eta}\mathrm{d}\eta. \tag{32}$$

Substituting (30)–(32) yields

$$\mathcal{D}^{h'}(v,r) = \mathcal{D}^h(v,r)(qt - p - jv) - q\mathcal{D}\mathrm{th}(v,r) \tag{33}$$

where $h' = \frac{\mathrm{d}h(t)}{\mathrm{d}t}$ and $th = t \cdot h(t)$.

1) Estimator Using One Partial Derivative: Assuming $\sigma_t \to \infty$, $q = ja_2$, and $p = ja_1$, thus [28]

$$\mathcal{D}^{h'}(v,r) = j\mathcal{D}^h(v,r)(a_2 t - a_1 - v) - ja_2\mathcal{D}\mathrm{th}(v,r). \tag{34}$$

Multiplying (34) by $(\mathcal{D}^h(v,r))^*$ and taking the real part reads

$$\hat{a}_2^{(t)}(v,r) = \frac{\Re\left(D^{h'}(v,r)\left(D^h(v,r)\right)^*\right)}{\Im\left(D^{th}(v,r)\left(D^h(v,r)\right)^*\right)}. \tag{35}$$

Since both the window derivative and the window multiplied by the time ramp result in ambiguity at the ridge of the target echo (see Fig. 2), the most useful part of the estimate is lost. In vast cases, especially in passive radars, a target usually occupies a single range–velocity cell; thus, the uncertainty at this point disables the possibility of precise acceleration estimation. Also, the assumption of a constant echo envelope cannot always be made. For these reasons, this estimator is not investigated in the further part of this work. However, one can use it in some applications as high-resolution radars, or in rough estimation with a reduced computational cost in the vicinity of the main target echo (the estimator needs only three RD maps to estimate the acceleration).

2) Estimator Using Two Partial Derivatives: The uncertainty effect graphically presented in Fig. 2 can be resolved using higher order window derivatives.

1) *Estimator Using Derivative with Respect to Time:* If the amplitude varies, (35) is biased [28]. Differentiating (33) with respect to time gives

$$\mathcal{D}^{h''}(v,r) = \mathcal{D}^{h'}(v,r)(qt - p - jv) - q\mathcal{D}^{th'}(v,r) \tag{36}$$

where $h'' = \frac{\mathrm{d}^2 h(t)}{\mathrm{d}t^2}$. Combining (33) and (36) into the linear systems yields

$$\hat{q}_t(v,r) = \frac{\mathcal{D}^{h''}(v,r)\mathcal{D}^h(v,r) - (\mathcal{D}^{h'}(v,r))^2}{\mathcal{D}^{h'}(v,r)\mathcal{D}\mathrm{th}(v,r) - \mathcal{D}^{th'}(v,r)\mathcal{D}^h(v,r)} \tag{37}$$

and the imaginary part of this equation gives the acceleration estimator as follows:

$$\hat{a}_2^{(t2)}(v,r) = \Im\left(\hat{q}_t(v,r)\right). \tag{38}$$

According to (37), the estimator requires five RD maps, and this value is constant and does not depend on processing parameters.

2) *Estimator Using Derivative with Respect to Velocity:* To compute the acceleration estimator with respect to velocity (frequency), one can assume

$$\frac{\partial \mathcal{D}^h(v,r)}{\partial v} = j\left(\mathcal{D}\mathrm{th}(v,r) - t\mathcal{D}^h(v,r)\right). \tag{39}$$

Differentiating (33) with respect to v once and combining into the linear system with (33) leads to $\hat{q}_v(v,r) =$

$$\frac{\mathcal{D}^{th'}{}_{(v,r)}\mathcal{D}^h{}_{(v,r)} + \left(\mathcal{D}^h{}_{(v,r)}\right)^2 - \mathcal{D}\mathrm{th}_{(v,r)}\mathcal{D}^{h'}{}_{(v,r)}}{\left(\mathcal{D}\mathrm{th}_{(v,r)}\right)^2 - \mathcal{D}^{t^2h}{}_{(v,r)}\mathcal{D}^h{}_{(v,r)}} \tag{40}$$

and

$$\hat{a}_2^{(tv)}(v,r) = \Im\left(\hat{q}_v(v,r)\right). \tag{41}$$

Estimator (41) requires five RD maps, the same as (37).

E. Final Estimate

Since $a_2 = \vartheta = 2\pi\frac{A}{\lambda}$, the acceleration for each (v,r) point can be estimated as

$$\hat{A}(v,r) = \frac{\hat{a}_2(v,r)\lambda}{2\pi} \tag{42}$$

where $\hat{a}_2(v,r)$ is given by (35), (38), or (41).

III. Implementation

The general concept of the proposed acceleration estimation process is presented in Fig. 3. In this specification, no distinction is made between the way range compression is performed, as it is a characteristic feature of a given radar and is independent of the proposed estimation concept. The input data are radar signals and the primary analysis window. Based on the radar signals, range compression is made, giving a range–time distribution. This result is passed to the RD map processor together with appropriately modified windows (e.g., window derivatives, window multiplied by the time ramp, etc.). An individual RD map is computed for each of these windows. Finally, based on the selected estimator, operations are performed following (35), (38), or (41). In general, any differentiable window is admissible (Gauss, Hamming, etc.). The Blackman–Harris window is used in this work because of its finite time support and simple form allowing efficient and analytical differentiation.

Simplified and high-level pseudocodes for the active and passive radar processing are listed in Algorithms 1 and 2, respectively. As mentioned, the only difference is in the range compression that is computed using the fast Fourier transform (FFT) algorithm in active radar, and using correlation in passive radars. As presented, the proposed estimation method can be integrated into a single block (a single method or function in software) of versatile usage and capable of migrating between different systems.

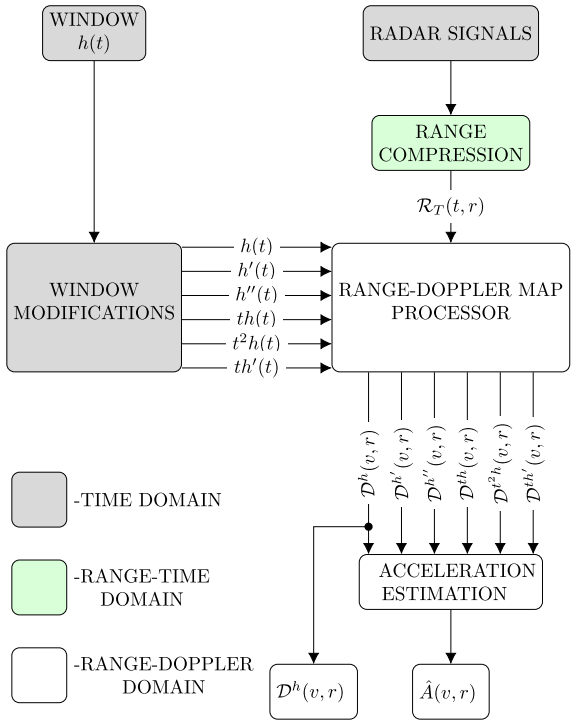

Fig. 3. Simplified flowchart of the proposed method.

IV. Reference Method

The proposed algorithm is compared against the reference method based on the concept of the matched filter [5], [20]. This method was chosen because it is unbiased and precisely estimates target acceleration. Other, more efficient methods usually assume some simplifications, such as uniform acceleration in forward scattering geometry [23]. The main goal of the comparison was to verify the proposed method efficacy comprising computation time reduction. Since known techniques are dedicated to solely active or passive radar, the comparison would be unreliable because, in each case, the computation would require separate processing. Thus, the comprehensive approach was applied. In the reference method, the signal after range compression $\mathcal{R}_T(t,r)$ is correlated with a template with certain values of a_1 and a_2 parameters

$$\mathcal{M}_T(r,a_1,a_2) = \int_{\mathbb{R}} \mathcal{R}_T(t,r) e^{-j\left(a_1 t + \frac{a_2 t^2}{2}\right)} \mathrm{d}t. \tag{43}$$

When the a_1 and a_2 parameters in the above equation match those in $\mathcal{R}_T(t,r)$, a high correlation peak occurs. By calculating $\mathcal{M}_T(r,a_1,a_2)$ for different values of r, a_1, and a_2, and searching for a maximum absolute value, an estimate of the correct values of r, a_1, and a_2 can be found.

In practice, the calculation of $\mathcal{M}_T(r,a_1,a_2)$ is performed on a discrete grid of r, a_1, and a_2. To prevent the discretization of the grid from limiting the estimation accuracy, the grid size should be appropriately small. This involves high computational complexity. Reduction of the computational burden can be achieved, e.g., using a finite impulse response filter in the velocity dimension [5].

Algorithm 1: Pseudocode for the Active Radar Acceleration Estimation.

```
Input:
    x % Beat signal vector
Define:
    fs % Sampling rate
    fc % Carrier frequency
    T_i % Integration time
    max_r % Maximum range
    max_v % Maximum frequency
    est % Selected estimator
Initialize arrays:
    X(max_r, T_i) % For x signal
    RC(max_r, T_i) % For range compression
Divide signal x into overlapping batches:
    X % Beat signal 2D matrix
Compute FFT of X along the fast time (range)
    RC = fft(X) % Range compression
Initialize arrays:
    RD(max_r, max_v)
    RDA(max_r, max_v)
Get needed windows of a length T_i for assumed est:
    h = window_generator(T_i, est)
for i ← 1 to max_r do
    Extract range cell: tmp = RC(i,:)
    Multiply tmp by required windows
    Compute FFT of each h and tmp product
    Store RD(i, :)
    Estimate acceleration using (35), (38), or (41)
    Scale the estimate according to (42)
    Store RDA(i, :)
end for
Return:
    RD % Range-Doppler map
    RDA % Range-Doppler acceleration map
```

Algorithm 2: Pseudocode for the Passive Radar Acceleration Estimation.

```
Input:
    x_r % Reference signal vector
    x_s % Surveillance signal vector
Define:
    fs % Sampling rate
    fc % Carrier frequency
    T_i % Integration time
    max_r % Maximum range
    max_v % Maximum frequency
    est % Selected estimator
Initialize arrays:
    X_r(max_r, T_i) % For x_r signal
    X_s(max_r, T_i) % For x_s signal
    RC(max_r, T_i) % For range compression
Divide signals x_r and x_s into overlapping batches:
    X_r % Reference signal 2D matrix
    X_s % Surveillance signal 2D matrix
Correlate X_r and X_s along the fast time (range)
    RC = xcorr(X_r, X_s)% Range compression
Initialize arrays:
    RD(max_r, max_v)
    RDA(max_r, max_v)
Get needed windows of a length T_i for assumed est:
    h = window_generator(T_i, est)
for i ← 1 to max_r do
    Extract range cell: tmp = RC(i,:)
    Multiply tmp by required windows
    Compute FFT of each product h and tmp
    Store RD(i, :)
    Estimate acceleration using (35), (38), or (41)
    Scale the estimate according to (42)
    Store RDA(i, :)
end for
Return:
    RD % Range-Doppler map
    RDA % Range-Doppler acceleration map
```

V. Simulations

The simulations presented in this section show the possibilities of the proposed estimators and how they can be illustrated. In addition, in-depth numerical analyses were conducted to estimate the numerical properties of the estimators in comparison to the technique from the literature.

A. Examples

Let us assume an FMCW radar working with a carrier frequency $f_c = 24$ GHz, bandwidth $B = 1$ GHz, sweep duration of 0.5 ms, and sweep repetition rate of 2 kHz. The radar illuminates a target at a distance $R = 50$ m moving with a velocity $V = 2$ m/s and acceleration $A = 0.5$ m/s^2. For simplicity of simulation, it was assumed that the target occupies a single range–velocity cell, and to comply with this assumption, the simulated acceleration is relatively low. The integration time was set to $T_i = 0.5$ s. The RD map and the range-Doppler acceleration (RDA) are shown in Fig. 4.[1] For the latter distribution, the estimator given by (38) was used as an example.

A single target is apparent on the RD map presented in Fig. 4(a). Its acceleration can be estimated using one of the

[1] In fact, the presented distributions depict the range–velocity maps. However, the RD nomenclature is more common in the radar community, and due to the direct relation between the Doppler shift and the velocity, in the rest of this article, the RD map corresponds to a signal distribution in range and velocity domains.

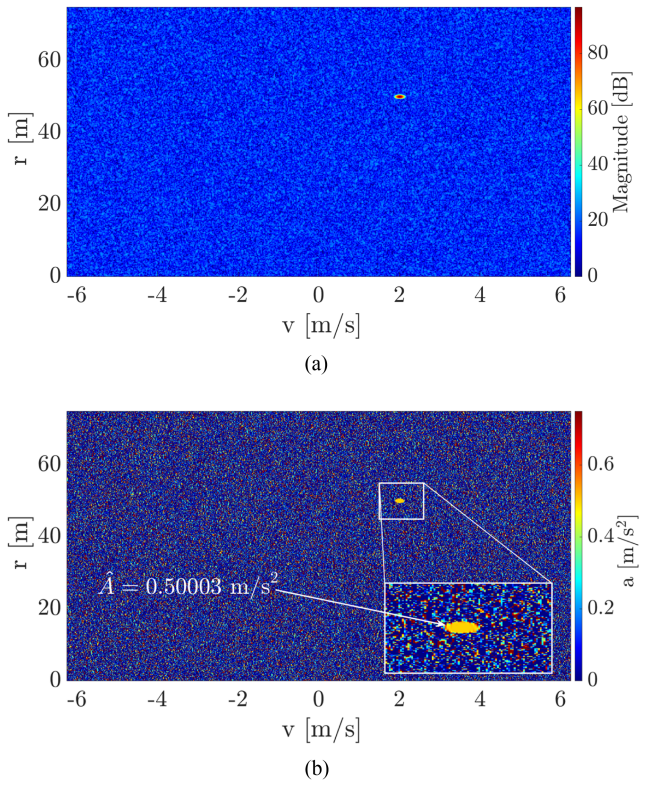

Fig. 4. FMCW radar simulation results. (a) Simulated RD map for an accelerating target. (b) Simulated RDA for an accelerating target.

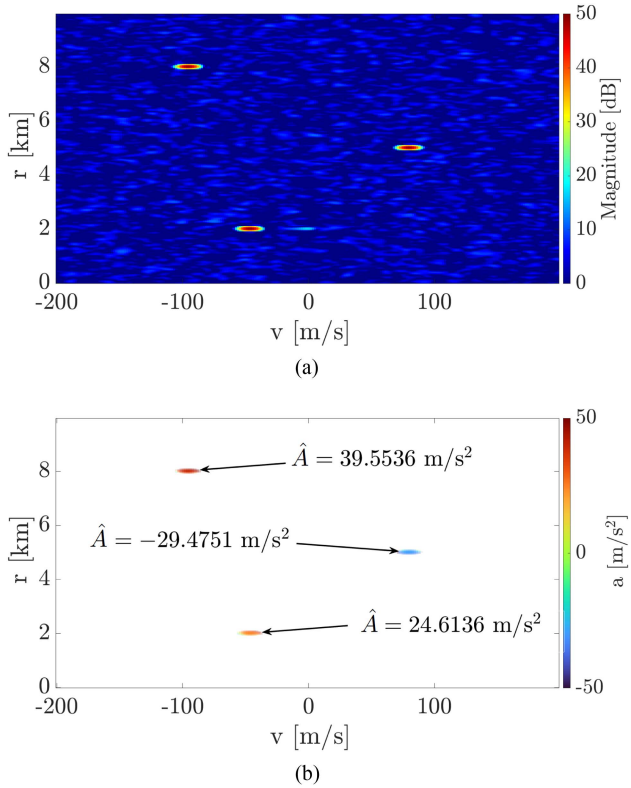

Fig. 5. Passive radar simulation results. (a) Simulated RD map for three accelerating targets. (b) Simulated RDA for three accelerating targets.

estimators proposed in Section II. As can be seen, the acceleration is estimated for each (v, r) coordinate. Therefore, aside from the estimate at the target point, the overall plane is covered by the estimated values corresponding to noise (this is why some estimated values are out of the analyzed scale). For the simulated target, $\hat{A} = 0.50003\ \mathrm{m/s^2}$, which is very close to the set value. The relative error is 0.006%, and results from the additive complex-valued white Gaussian noise added to signals. Comprising the integration gain that is defined as

$$G_i = BT_i \tag{44}$$

where B is the signal bandwidth, and the SNR was approximately equal to 60 dB. In this and all further cases, the estimation value is read at the point of the strongest energy on the RD map, which can be simply adopted in real-life systems where the constant false alarm rate (CFAR) algorithms are usually implemented. However, in practice, our interest is to find a target parameter (or several targets), and the target surroundings can be neglected. To make the RDA more readable, one can use a saturated RDA, where the magnitude of the RD map governs the distribution saturation. Such an illustrative approach is used in the further part of this work to focus only on the target vicinity.

The second example comprises the multitarget passive radar scenario. For the carrier frequency $f_c = 680$ MHz and a bandwidth $B = 7.6$ MHz, three targets have the following parameters.

1) $R_1 = 5$ km, $V_1 = 80$ m/s, $A_1 = -30$ m/s^2.
2) $R_2 = 2$ km, $V_2 = -40$ m/s, $A_2 = 25$ m/s^2.
3) $R_3 = 8$ km, $V_3 = -100$ m/s, $A_3 = 40$ m/s^2.

The simulation was carried out for the integration time $T_i = 0.1$ s. The RD map and the saturated RDA are depicted in Fig. 5. In this case, the estimator (41) was used as an example. Three targets are visible, as established in the simulation setup. The acceleration was estimated and shown in Fig. 5(b) for each of them. Also, only the targets that contribute the most are visible, thanks to the saturated distribution. The estimation error does not exceed 2%, and the computed values coincide with the set ones.

A precious property of the proposed method is that increasing the number of targets does not affect the computational effort. The computational complexity is constant and is not related to the presence of additional objects. The reference method requires many more RD maps to be determined, yet it may turn out that the object acceleration is outside the scanned range. Then, the computational complexity is a tradeoff between accuracy and processing time.

B. Numerical Stability Assessment

The simulations were conducted to quantitatively compare the proposed approach and the reference method. Since the range compression in active and passive radars can be approximated in the same way as shown in Section II, for simplicity, the simulations were performed only for the passive radar. A single target at a bistatic range $R = 4$ km, velocity $V = 50$ m/s, and acceleration $A = 20$ m/s^2 was illuminated by the signal with a carrier frequency $f_c = 680$ MHz, a bandwidth $B = 1$ MHz, and an integration time $T_i = 200$ ms. According to (44), the integration gain was $G_i = 53$ dB. The target echo power was -40 dB. For estimators (38) and (41), and for the reference method [5],

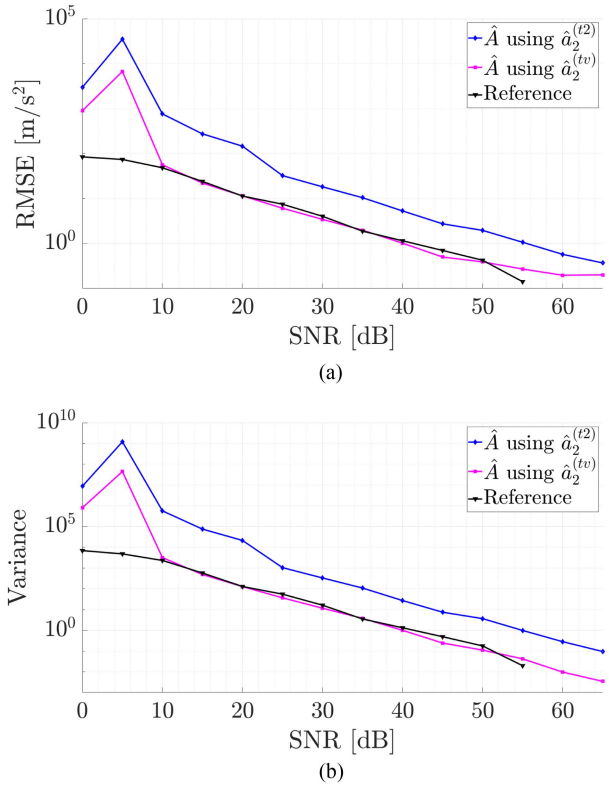

Fig. 6. Statistical properties of the estimators. (a) RMSE. (b) Variance.

the noise-like illuminating signal (imitating, e.g., an OFDM waveform) was simulated for different SNR values: SNR $= \{0, 5, 10, 15, 20, 25, 30, 35, 40, 45, 50, 55, 60, 65\}$ dB with an additive complex-valued white Gaussian noise assumption. The SNR is defined as a ratio of the target echo to the noise level comprising the integration gain G_i. The processing was done for the RD map with 33 range cells from 0 to 10 km and 902 velocity cells from -500 to 500 m/s. For the reference method, the space of considered acceleration was spread from -100 to 100 m/s^2 and divided into 201 points, yielding 1 m/s^2 spacing. The acceleration was estimated in 100 Monte Carlo simulations repeated for each estimator and each SNR value. The root-mean-square error (RMSE) and the variance are shown in Fig. 6.

As can be seen, variance and RMSE drop with the SNR for all methods in question. Estimator (41) is more accurate and has less variance than (38) and is comparable to the reference method for SNR ≥ 10 dB. Estimator (38) is characterized by inferior numerical stability. However, experiments conducted by the authors show that it can also be used in practical applications as an initial or rough estimation step with an error negligible in some cases. Its usefulness is shown in the real-life data analysis presented in the next section. The reference method is perfect for SNR ≥ 55 dB, and its variance and error are invisible in the logarithmic scale since they are equal to 0.

C. Computational Complexity

Before moving to real-life data analysis, let us consider the computational efficiency of the proposed estimators. Fig. 7 shows the results of processing time for the considered methods

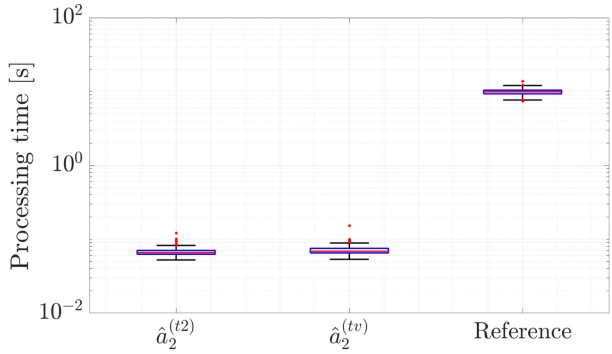

Fig. 7. Processing time. The mean values for $\hat{a}_2^{(t2)}$, $\hat{a}_2^{(tv)}$, and for the reference method are 69.1 ms, 71.6 ms, and 9.93 s, respectively.

from 100 Monte Carlo simulations.[2] The implementation of the RD map computation was the same for the proposed and the reference methods. The processing parameters were identical to those listed at the beginning of this section and equal for both algorithms. The results clearly show the superiority of the proposed estimators from the processing time perspective. The mean value for estimators (38) and (41) was approx. 140 times shorter than for the reference technique. Moreover, the processing time can be extended for a wider or more dense space of accelerations for the technique from [5].

Let us assume the FFT complexity in the Landau notation as $\mathcal{O}(N \log_2 N)$, where N is the Fourier transform size [36]. For the RD map computation, the algorithm is performed for each range cell, and let us denote their number with M. Hence, the computational complexity of the entire RD map can be expressed as $\mathcal{O}(MN \log_2 N)$. The reference method needs K such RD maps (each with a modulated reference signal; K is usually from dozens to hundreds), so the complexity of the processing becomes $\mathcal{O}(KMN \log_2 N)$. For the method proposed in this article, the complexity is constant $\mathcal{O}(5MN \log_2 N)$. In total, 5 is the number of unique RD maps computed with a specific window (e.g., its derivative or multiplied by the time ramp) as stated in (38) and (41). For two values of K considered in this article, namely $K = 100$ and $K = 1000$, the complexity cost reduction equals 20 and 200, respectively. The same conclusions stem from the processing time comparison.

VI. Real-Life Data Analysis

A. Active Radar

For the active radar experiment, the XY-DemoRad system developed by XY-Sensing Ltd. was used [37]. The sensor is presented in Fig. 8. The radar recorded the drone (XIRO Xplorer) echo using a signal bandwidth $B = 1$ GHz (corresponding to 15 cm range resolution), carrier frequency $f_c = 24$ GHz, and a sweep repetition rate of 2 kHz. The signal was processed offline, and the drone acceleration was estimated using the estimator (38). The integration time was set to $T_i = 0.5$ s. The results are presented in Fig. 9.

[2]For computation, the MATLAB 2021a environment was used, CPU Intel i7-9750H 2.6 GHz, 32 GB DDR4, SSD drive, Windows 10.

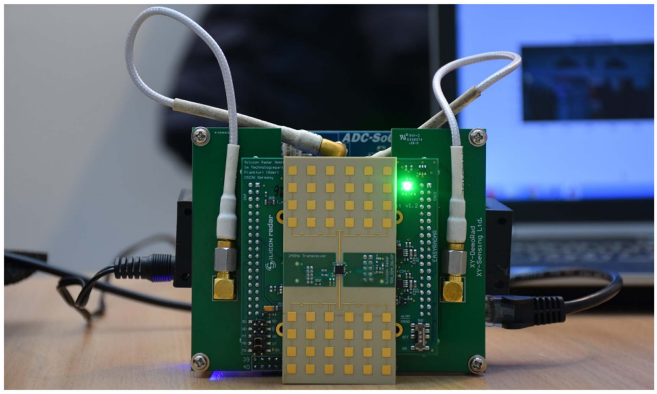

Fig. 8. FMCW radar used in the real-life experiment.

The target is apparent at the range $R = 22.76$ m and the velocity $V = 1.95$ m/s. Its acceleration at the point of the maximum energy was estimated as $\hat{A} = 0.335296$ m/s^2 using the proposed method. A 3-D cube was computed for the reference technique and is shown in Fig. 9(c). As presented, the range in which the target acceleration was searched was spanned within $A \in (-5, 5)$ m/s^2. The cross section across the range cell with a target echo is presented in Fig. 9(d). A precise estimate was read as a hill's peak from Fig. 9(e). The assessed acceleration equals $\hat{A} = 0.35$ m/s^2, which is very close to the value estimated using (38). Unfortunately, the additional measurements comprising inertial or GPS sensors were not conducted in this case. However, assuming that the correct acceleration value is $A = 0.35$ m/s^2, the error between the reference and the proposed method is 4.2%. The processing time for the proposed technique was 45 ms, while for the reference one it was 1.74 s for 101 points and 17.3 s for 1001 points of the acceleration axis for the same computing machine as in the simulations.

Due to the lack of the additional reference as a GPS or inertial data, a double-check validation was conducted. The analyzed signal was of length $T_i = 0.5$ s. Thus, to confirm that within the observation time, given that the target's velocity varies in relation to the estimated value, the signal was separated into two equally long parts allowing for the computation of two RD maps with $T_i = 0.25$ s. By analyzing the velocity of the drone in the first and the second result, it was possible to verify the acceleration estimate precision. The outcomes are shown in Fig. 10. In Fig. 10(a), the first RD map can be seen. From the result, one can deduce that the target is at the range $R_{t1} = 22.62$ m and moves with a velocity of $V_{t1} = 1.91$ m/s. For the second snapshot, $R_{t2} = 23.03$ and $V_{t2} = 1.99$ m/s. Assuming the estimated acceleration $\hat{A} = 0.335296$ m/s^2, the velocity in the second snapshot should be $\hat{V}_{t2} = 1.91$ m/s $+ 0.25$ s $\cdot\, 0.335296$ m/s^2 $=$ 1.9938 m/s, which corresponds to $V_{t2} = 1.99$ m/s.

To make sure that the drone's blades do not affect the estimate, the example from Section V-A was modified. Namely, the simulated echo of blades (with the amplitude $10\times$ weaker than the main echo) was added to the signal. The RD and RDA maps are depicted in Fig. 11. The classical RD map exhibits an apparent influence of the rotors, which can be seen as a

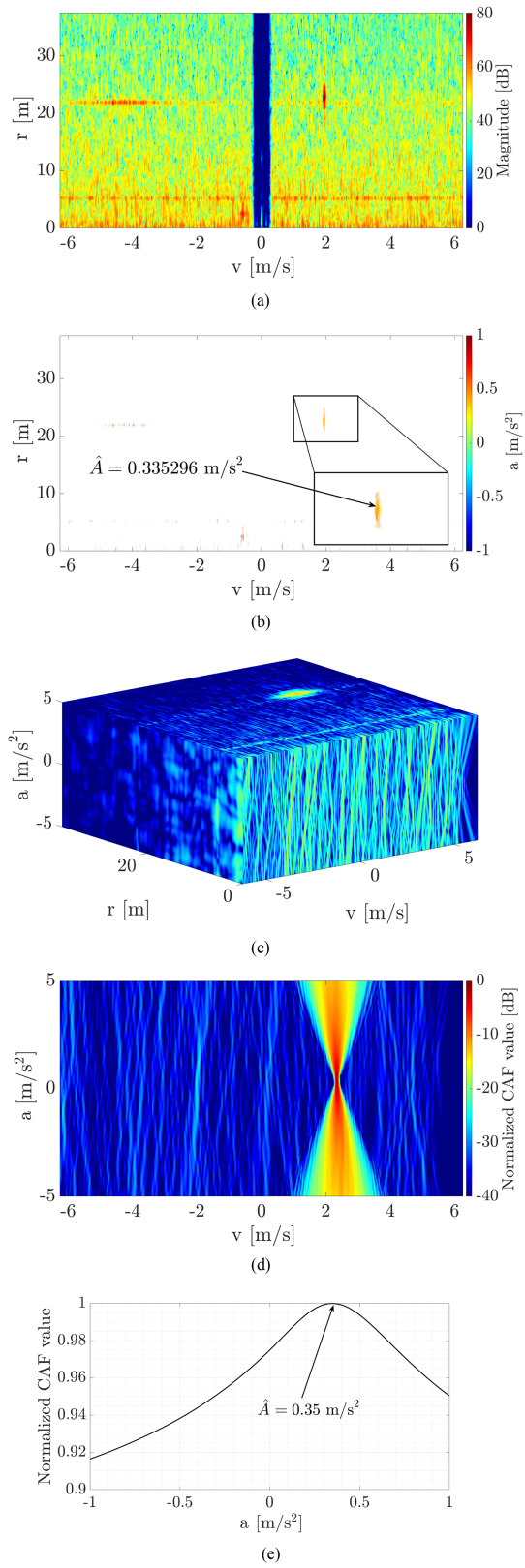

Fig. 9. FMCW radar real-life data processing results. (a) Real-life RD map for a single accelerating drone. (b) Real-life RDA for a single accelerating drone. (c) RD acceleration cube. (d) Cross section across the range plane containing a target echo for different acceleration values. (e) Cross section across the range and velocity cell containing a target echo for different acceleration values.

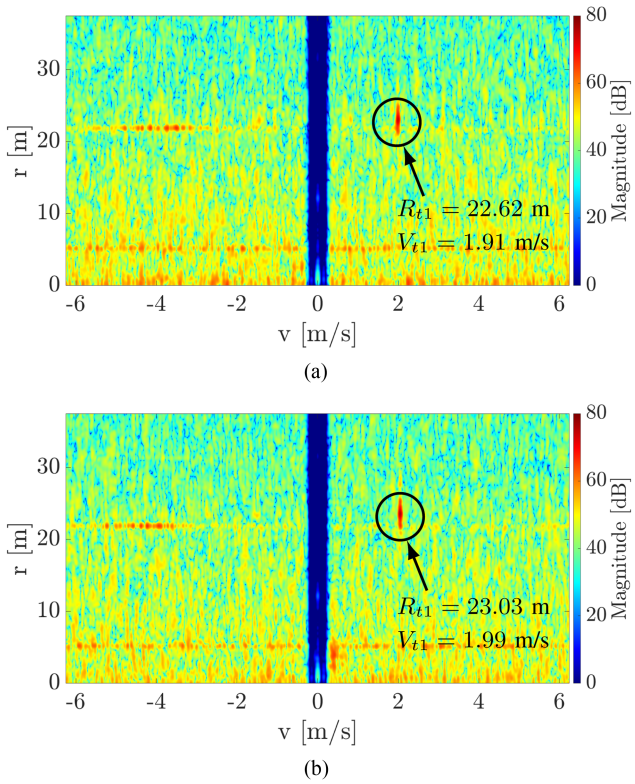

Fig. 10. Verification results of acceleration estimation in active radar. The RD maps were obtained by dividing the initial signal into two segments, and then the processing was conducted on each segment separately. (a) Real-life RD map for a single accelerating drone—first snapshot. (b) Real-life RDA for a single accelerating drone—second snapshot.

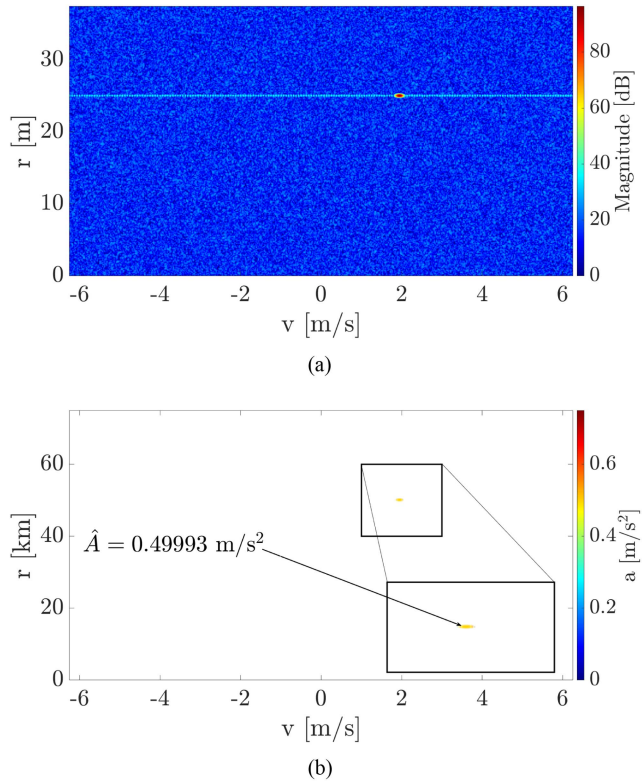

Fig. 11. Analysis of the drone's blades influence of the main body acceleration estimate. (a) RD map for the simulated drone. (b) RDA map for the simulated drone.

typical wideband spectrum spread at the range where the target is observed. The effect is typical for drones, helicopters, etc. The estimate, however, is not affected by this issue as the blades' echo occupies separate velocity cells. Because the proposed acceleration estimation is carried out in each (r, v) location separately, one can differentiate between the main body of the drone and its blades. The negligible difference between the outcome in Figs. 11(b) and 4(b) originates from the noise added to the signal and does not contribute significantly to the final result. Thus, it can be concluded that the drone's acceleration was correctly estimated, and the influence of its blades can be ignored.

B. Passive Radar

The real-life signal originates from the PaRaDe passive radar system [5], [38]. The illuminator of opportunity was an FM radio transmitter with the carrier frequency $f_c = 83.2$ MHz and the bandwidth $B = 50$ kHz. The radar observed a maneuvering jet fighter, and the signals (reference—from the antenna pointed toward the transmitter and surveillance—from the antenna directed toward the space) were filtered, sampled, and recorded. The processing was performed offline. A sample snapshot was selected for further processing, and the results are illustrated in Fig. 12 for the integration time $T_i = 0.5$ s.

The jet fighter is visible at $R = 41.5$ km and $V = -185.6$ m/s, as shown in Fig. 12(a). The saturated RDA using (41) is shown in Fig. 12(b) where the acceleration was estimated as $\hat{A} = 38.1422$ m/s^2. The outcome was compared with the reference method. The whole 3-D RD distribution with the acceleration set $A \in (-1000, 1000)$ m/s^2 and its cross section along the range cell with a target are shown in Fig. 12(c) and (d), respectively. The final estimate was the one shown in Fig. 12(e) as the maximum value of the 3-D distribution for the particular range and velocity bin and equals $\hat{A} = 36.7$ m/s^2. Both estimated values are very close and coincide with the acceleration calculated from the difference of velocities [5]. Assuming the acceleration estimated using the reference method is ideal, the estimation error is 3.94%. However, there are significant deviations in processing time. The processing time for the reference method with 2001 points was 101.1 s. Reduction of the space to 201 points allowed for the outcome to be obtained in 8.5 s. The estimate was computed after 54 ms with a comparable result for the proposed method (the processing was carried out using the same computing machine as in the simulations).

A double-check validation was performed in the same way as for the active radar scenario. The outcomes are delineated in Fig. 13 and presented two RD maps for $T_i = 0.25$ s instead of the initial value 0.5 s. From Fig. 10(a), one can read the target parameters as $R_{t1} = 41.5$ km and $V_{t1} = -190.24$ m/s. In the second snapshot, one has $R_{t2} = 41.5$ km (due to the low resolution, the target was in the same range cell) and $V_{t2} = -176.65$ m/s. Assuming the estimated acceleration, one can obtain $\hat{V}_{t2} = -190.24$ m/s $+ 0.25$ s $\cdot 38.1422$ m/s$^2 = -180.7124$ m/s, which is close to V_{t2} with the difference less than 4 m/s (in the processing, the velocity resolution was about 6.8 m/s so the difference is negligible). It has to be noted that during the flight,

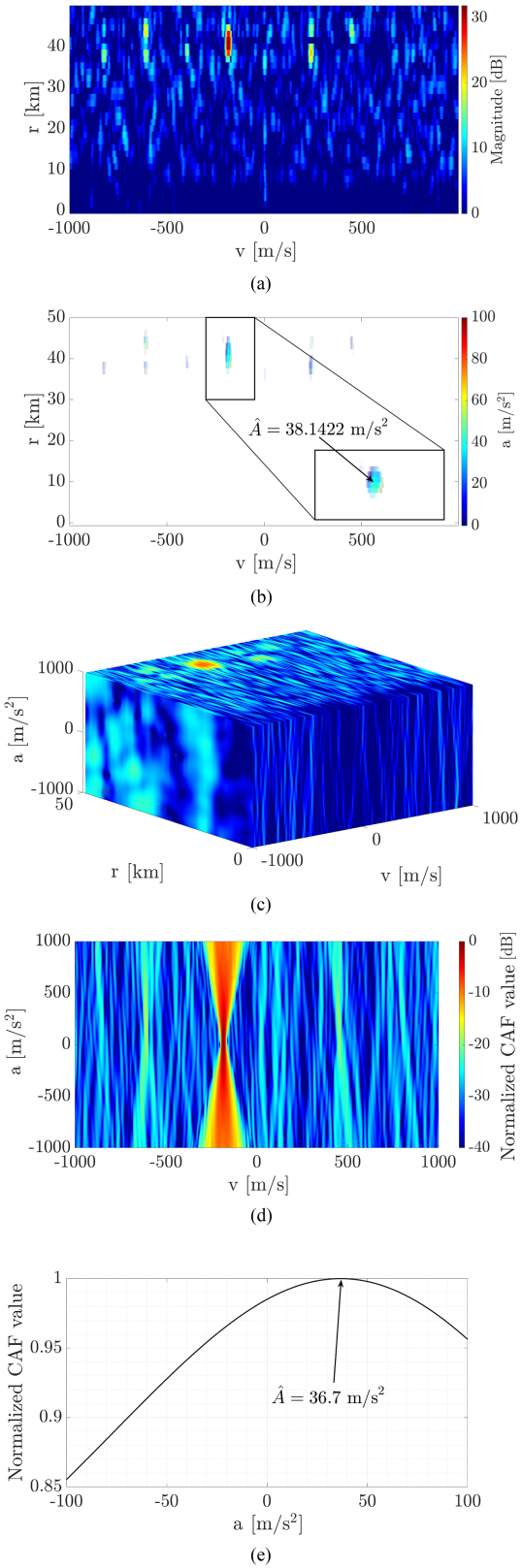

Fig. 12. PCL radar real-life data processing results. (a) Real-life RD map for an accelerating jet fighter. (b) Real-life RDA for an accelerating jet fighter. (c) RD-acceleration cube. (d) Cross section across the range plane containing a target echo for different acceleration values. (e) Cross section across the range and velocity cell containing a target echo for different acceleration values.

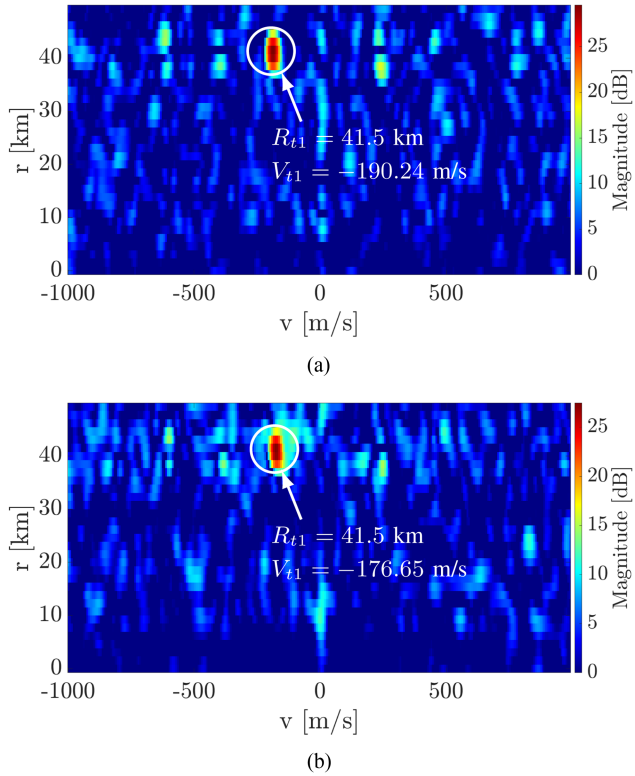

Fig. 13. Verification results of acceleration estimation in passive radar—two RD maps with a smaller integration time. (a) Real-life RD map for a maneuvering jet fighter—first snapshot. (b) Real-life RDA for a maneuvering jet fighter—second snapshot.

the jet fighter was maneuvering; thus, the estimate can be slightly biased due to the higher order kinematic parameters.

VII. Application to Integration Time Elongation

Rapid acceleration entails target echo blurring on the RD map [5]. Assuming that the target has acceleration A, the velocity change during the integration time T_i is

$$\delta V = T_i \cdot A. \tag{45}$$

If the velocity changes, δV is significant with respect to the velocity resolution cell ΔV, and velocity cell migration occurs. The velocity resolution cell can be calculated as follows:

$$\Delta V = \frac{\lambda}{M \cdot T_i} \tag{46}$$

where λ is the wavelength, and M is a coefficient equal to 1.0 for bistatic and 2.0 for monostatic radar. Therefore, the limitation on the integration time for a given acceleration can be formulated as

$$T_i < \sqrt{\frac{\lambda}{C \cdot A}}. \tag{47}$$

If the above condition is not met, echo spreading across the velocity dimension can be expected. The longer the integration time, the more apparent the echo spread on the map. One can modulate the reference signal according to the estimated

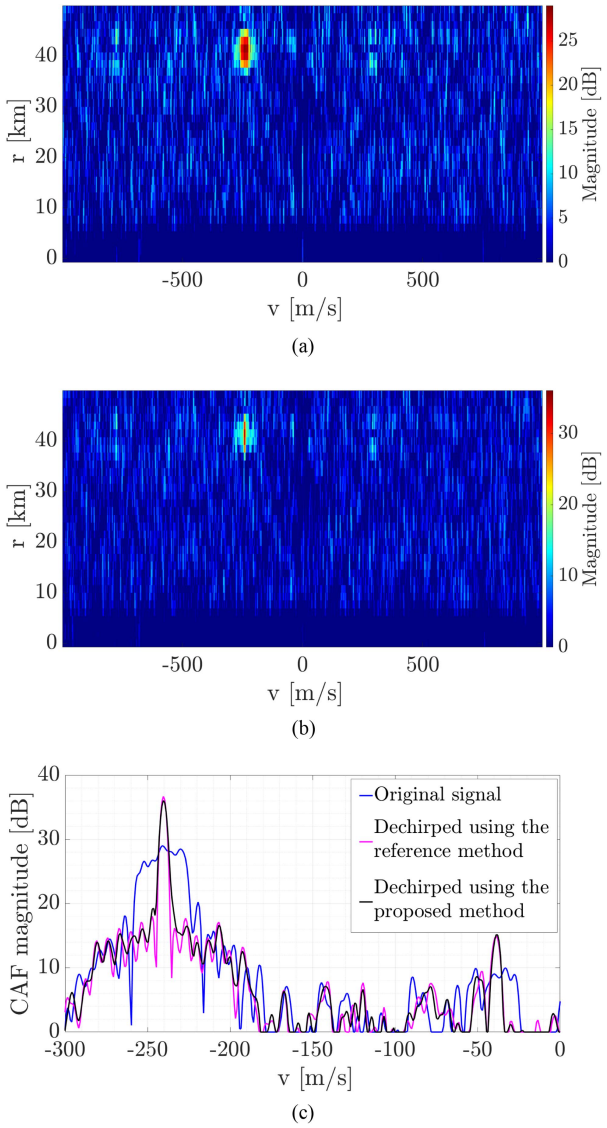

Fig. 14. Illustration of the target acceleration influence on the RD map. (a) RD map for $T_i = 2$ s with the original reference signal. (b) RD map for $T_i = 2$ s with the dechirped reference signal. (c) CAF cross section through the range cell with a target before and after reference modulation.

acceleration to compensate for the acceleration and focus the target echo in a particular range and Doppler bin

$$x_T^d(t) = x_T(t)e^{-j\frac{\hat{a}_2 t^2}{2}}. \tag{48}$$

where $\hat{a}_2$ is the estimate of the target's acceleration. The dechirped reference signal is then processed in the same way as in classical RD processing. As a result, one can gain several benefits. First, the integration time can be elongated. This results in an increase in the integration gain (44). When the target echo migrates between the resolution cells, the obtained gain is reduced [39]. Second, the dechirped reference increases the CAF value, yielding better detection capabilities. Third, the velocity can be estimated more precisely since the target echo is concentrated in a particular RD coordinate. Fig. 14 illustrates the consequence of excessive integration time and the solution offered by the acceleration estimation.

Increasing the integration time from 0.5 to 2 s caused an apparent stretch of the target echo, as shown in Fig. 14(a). The velocity estimation becomes more difficult due to the occupancy of several Doppler cells. Moreover, the signal energy is dispersed, and the peak height also decreases. The target acceleration estimated in Section VI-B served as a value of FM of the reference signal. After dechirping the signal, the RD map is characterized by a strong target echo in a single RD bin, as presented in Fig. 14(b). The peak is higher and more focused, making the detection process more robust. In Fig. 14(c), cross sections of three RD maps are superimposed. Without the reference signal demodulation, the target takes several Doppler bins from -225 to -260 m/s, and unambiguous velocity estimation is impossible. After considering a meaningful acceleration, the peak value increased by approx. 7 dB. The difference between the peak value after the reference signal dechirping using the estimate computed using the proposed and the reference method is 0.348 dB. Such a difference can be ignored if one compares the processing time that is significantly shorter for the proposed technique. The target velocity can be estimated as $V = -240.45$ m/s, which is impossible without the reference signal modulation.

VIII. Discussion

In the entire article, the processing was conducted under a prerequisite that the range migration does not occur. In some practical applications, especially in high-resolution radars, this effect is common, and the only way to avoid it is to shorten the integration time. In turn, this entails a lower integration gain [see (44)], thus disabling smaller targets (to be precise, with a lower radar cross section) to be detected. If the acceleration is constant and the integration time is sufficiently long for the range migration to occur, the proposed estimators will be able to return a correct estimate. This is because the estimate is computed for each (r, v) coordinate. Thus, one can obtain the outcome for the target shifted in range and velocity. When the acceleration varies, the estimated acceleration will be biased (a so-called jerk and snap can occur, thus disturbing the estimate), but this is a problem beyond the scope of this work as it comprises higher order target kinematic parameter estimation.

The main advantage of the proposed method is that it does not require any modifications to existing systems other than its implementation using already available tools. Estimating targets' accelerations can be incorporated into the radar signal processing block so that target detection works simultaneously with acceleration estimation. Consequently, the proposed method does not require additional detection techniques or thresholding since targets are detected in the same RD domain using typical algorithms, such as CFAR. Therefore, the acceleration estimation of a particular object comes down to reading the estimate from the RDA in the same coordinate as the CFAR algorithm returns detection.

IX. Conclusion

In this article, a novel method for estimating vehicle acceleration has been proposed. The technique can be applied to different types of radar, such as active monostatic FMCW radar and passive bistatic radar. This results from the fact that

intermediate calculation results have a very similar form. Also, the technique should work for pulse and noise radars since the received signal model there is very similar to the one analyzed in this article. The numerical experiments showed that the method's performance, while not as good as the reference method, is still excellent, especially for high SNR values (greater than 10 dB). The advantage of using the proposed approach is a reduction of the computational complexity in comparison with the reference method. In particular, similar accuracy can be obtained by reducing the computational complexity by two orders of magnitude. The method was successfully applied to simulated and real-life data for both FMCW and passive radars. This fact allows one to assume that this approach can be adapted to other types of radar.

In the future, the authors plan to derive higher order kinematic parameter estimators, such as jerk and snap. As a result, a whole family of estimators can be obtained, allowing for target parameterization for classification and tracking improvement. Also, a profound analysis of the clutter and interference influence on estimators' efficiency should be inspected. Especially, the problem of slow-moving targets in the background of clutter and the impact of intentional and unintentional interferences should be addressed, which is the plan for further investigation.

References

[1] M. P. Jarabo-Amores et al., "Drone detection feasibility with passive radars," in *Proc. IEEE 15th Eur. Radar Conf.*, 2018, pp. 313–316.

[2] C. Clemente, F. Fioranelli, F. Colone, and G. Li, *Radar Countermeasures for Unmanned Aerial Vehicles*, (Series Radar, Sonar and Navigation). London, U.K.: Institution of Engineering and Technology, 2021.

[3] T. Yang, A. D. Maio, J. Zheng, T. Su, V. Carotenuto, and A. Aubry, "An adaptive radar signal processor for UAVs detection with super-resolution capabilities," *IEEE Sensors J.*, vol. 21, no. 18, pp. 20778–20787, Sep. 2021.

[4] M. Rosamilia, A. Balleri, A. D. Maio, A. Aubry, and V. Carotenuto, "Radar detection performance prediction using measured UAVs RCS data," *IEEE Trans. Aerosp. Electron. Syst.*, vol. 59, no. 4, pp. 3550–3565, Aug. 2023.

[5] M. Malanowski, "Detection and parameter estimation of manoeuvring targets with passive bistatic radar," *IET Radar, Sonar Navigation*, vol. 6, pp. 739–745, Oct. 2012.

[6] J. Palmer, S. Palumbo, A. Summers, D. Merrett, S. Searle, and S. Howard, "An overview of an illuminator of opportunity passive radar research project and its signal processing research directions," *Digit. Signal Process.*, vol. 21, no. 5, pp. 593–599, 2011.

[7] M. Malanowski, K. Borowiec, and S. Rzewuski, "Rocket detection using passive radar - challenges and solutions," in *Proc. IEEE Int. Conf. Radar*, 2018, pp. 1–5.

[8] R. Zhang, Y. Wang, C. Yeh, and X. Lu, "Precession parameter estimation of warhead with fins based on micro-Doppler effect and radar network," *IEEE Trans. Aerosp. Electron. Syst.*, vol. 59, no. 1, pp. 443–459, Feb. 2023.

[9] J. E. Palmer, H. A. Harms, S. J. Searle, and L. M. Davis, "DVB-T passive radar signal processing," *IEEE Trans. Signal Process.*, vol. 61, no. 8, pp. 2116–2126, Apr. 2013.

[10] J. Liu, H. Li, and B. Himed, "Two target detection algorithms for passive multistatic radar," *IEEE Trans. Signal Process.*, vol. 62, no. 22, pp. 5930–5939, Nov. 2014.

[11] Z. Wang, Q. He, and R. S. Blum, "Exploiting information about the structure of signals of opportunity for passive radar performance increase," *IEEE Trans. Signal Process.*, vol. 69, pp. 6083–6100, 2021, doi: 10.1109/TSP.2021.3099627.

[12] C. R. Berger, B. Demissie, J. Heckenbach, P. Willett, and S. Zhou, "Signal processing for passive radar using OFDM waveforms," *IEEE J. Sel. Topics Signal Process.*, vol. 4, no. 1, pp. 226–238, Feb. 2010.

[13] F. Wang, H. Li, X. Zhang, and B. Himed, "Signal parameter estimation for passive bistatic radar with waveform correlation exploitation," *IEEE Trans. Aerosp. Electron. Syst.*, vol. 54, no. 3, pp. 1135–1150, Jun. 2018.

[14] C. Zhang, S. Shi, S. Yan, and J. Gong, "Moving target detection and parameter estimation using BeiDou GEO satellites-based passive radar with short-time integration," *IEEE J. Sel. Topics Appl. Earth Observ. Remote Sens.*, vol. 16, pp. 3959–3972, 2023, doi: 10.1109/JSTARS.2023.3266875.

[15] C. Huang, Z. Li, H. An, Z. Sun, J. Wu, and J. Yang, "Optimal GNSS-Based passive SAR large field-of-view imaging via multistatic configuration: Method and experimental validation," *IEEE J. Sel. Topics Appl. Earth Observ. Remote Sens.*, vol. 15, pp. 9873–9884, 2022, doi: 10.1109/JSTARS.2022.3221214.

[16] P. Wang, X. Zhou, Y. Fang, H. Zeng, and J. Chen, "GNSS-Based passive inverse SAR imaging," *IEEE J. Sel. Topics Appl. Earth Observ. Remote Sens.*, vol. 16, pp. 508–521, 2023, doi: 10.1109/JSTARS.2022.3225832.

[17] K. S. Kulpa and J. Misiurewicz, "Stretch processing for long integration time passive covert radar," in *Proc. IEEE CIE Int. Conf. Radar*, 2006, pp. 1–4.

[18] X. Li, G. Cui, W. Yi, and L. Kong, "Radar maneuvering target detection and motion parameter estimation based on TRT-SGRFT," *Signal Process.*, vol. 133, pp. 107–116, 2017.

[19] K. Borowiec and M. Malanowski, "Accelerating rocket detection using passive bistatic radar," in *Proc. IEEE 17th Int. Radar Symp.*, 2016, pp. 1–5.

[20] M. Malanowski, K. Kulpa, and J. Misiurewicz, "Acceleration estimation for passive coherent location radar," in *Proc. IEEE Radar Conf.*, 2008, pp. 1–5.

[21] Z. Solatzadeh and A. Zaimbashi, "Accelerating target detection in passive radar sensors: Delay-Doppler-acceleration estimation," *IEEE Sensors J.*, vol. 18, no. 13, pp. 5445–5454, Jul. 2018.

[22] S. Subedi, Y. D. Zhang, M. G. Amin, and B. Himed, "Robust motion parameter estimation in multistatic passive radar," in *Proc. IEEE 21st Eur. Signal Process. Conf.*, 2013, pp. 1–5.

[23] X. Ai, Y. Zheng, Z. Xu, and F. Zhao, "Parameter estimation for uniformly accelerating moving target in the forward scatter radar network," *Remote Sens.*, vol. 14, no. 4, 2022, Art. no. 1006.

[24] P. Huang, G. Liao, Z. Yang, X.-G. Xia, J.-T. Ma, and J. Ma, "Long-time coherent integration for weak maneuvering target detection and high-order motion parameter estimation based on keystone transform," *IEEE Trans. Signal Process.*, vol. 64, no. 15, pp. 4013–4026, Aug. 2016.

[25] X. Li, G. Cui, L. Kong, and W. Yi, "Fast non-searching method for maneuvering target detection and motion parameters estimation," *IEEE Trans. Signal Process.*, vol. 64, no. 9, pp. 2232–2244, May 2016.

[26] X. Lv, G. Bi, C. Wan, and M. Xing, "Lv's distribution: Principle, implementation, properties, and performance," *IEEE Trans. Signal Process.*, vol. 59, no. 8, pp. 3576–3591, Aug. 2011.

[27] H. Lin, C. Zeng, H. Zhang, and G. Jiang, "Radar maneuvering target motion parameter estimation based on Hough transform and polynomial Chirplet transform," *IEEE Access*, vol. 9, pp. 35178–35195, 2021.

[28] D. Fourer, F. Auger, K. Czarnecki, S. Meignen, and P. Flandrin, "Chirp rate and instantaneous frequency estimation: Application to recursive vertical synchrosqueezing," *IEEE Signal Process. Lett.*, vol. 24, no. 11, pp. 1724–1728, Nov. 2017.

[29] R. Alaifari and M. Wellershoff, "Uniqueness of STFT phase retrieval for bandlimited functions," *Appl. Comput. Harmon. Anal.*, vol. 50, pp. 34–48, 2021.

[30] J. J. Benedetto, I. Konstantinidis, and M. Rangaswamy, "The role of the ambiguity function in waveform design and phase coded waveforms," 2008.

[31] M. I. Skolnik, *Radar Handbook*. New York, NY, USA: McGraw-Hill, 1970.

[32] H. Kuschel, D. Cristallini, and K. E. Olsen, "Tutorial: Passive radar tutorial," *IEEE Aeros. Electron. Syst. Mag.*, vol. 34, no. 2, pp. 2–19, Feb. 2019.

[33] R. Rytel-Andrianik, "On the ambiguity function for accelerating target in FMCW radar," in *Proc. Int. Conf. Microw., Radar Wireless Commun.*, 2006, pp. 207–210.

[34] C. Moscardini, D. Petri, A. Capria, M. Conti, M. Martorella, and F. Berizzi, "Batches algorithm for passive radar: A theoretical analysis," *IEEE Trans. Aerosp. Electron. Syst.*, vol. 51, no. 2, pp. 1475–1487, Apr. 2015.

[35] R. Behera, S. Meignen, and T. Oberlin, "Theoretical analysis of the second-order synchrosqueezing transform," *Appl. Comput. Harmon. Anal.*, vol. 45, no. 2, pp. 379–404, 2018.

[36] E. Rajaby and S. M. Sayedi, "A. structured review of sparse fast Fourier transform algorithms," *Digit. Signal Process.*, vol. 123, 2022, Art. no. 103403.

[37] P. Samczynski, K. Stasiak, D. Gromek, K. Kulpa, and J. Misiurewicz, "XY-DemoRad–Novel K- and mm-band radar demo kit for educational and commercial applications," in *Proc. IEEE 20th Int. Radar Symp.*, 2019, pp. 1–11.

[38] M. Malanowski, K. Kulpa, and J. Misiurewicz, "PaRaDe - PAssive RAdar DEmonstrator family development at Warsaw University of Technology," in *Proc. Microw., Radar Remote Sens. Symp.*, 2008, pp. 75–78.

[39] M. Malanowski and K. Kulpa, "Analysis of integration gain in passive radar," in *Proc. IEEE Int. Conf. Radar*, 2008, pp. 323–328.